

Facile synthesis of CuInS₂/ZnS quantum dots with highly near-infrared photoluminescence via phosphor-free process

Ruili Zhang · Ping Yang · Yiqian Wang

Received: 27 March 2013 / Accepted: 31 July 2013
© Springer Science+Business Media Dordrecht 2013

Abstract We present the synthesis of CuInS₂ quantum dots (QDs) with a size range of 3–4 nm through a phosphor-free method. The photoluminescence (PL) properties of CuInS₂ QDs synthesized using various Cu/In molar ratios were investigated. With the decrease of Cu/In molar ratio, the PL peak wavelength revealed a clear blue shift by ca. 100 nm and a noticeable increase in PL intensity. Being coated with a ZnS shell on CuInS₂ QDs, the resulting core/shell QDs exhibited a dramatic increase of PL efficiency and stability, with the maximum PL efficiency up to 39 %. This is ascribed to the efficient reduction of non-radiative recombination after surface modification. In addition, the PL peak wavelengths were tuned from 670 to 800 nm. The transmission electron microscopy observation and X-ray diffraction analysis indicated that the CuInS₂ and CuInS₂/ZnS QDs revealed a “dot” shaped morphology and exhibited a wurtzite structure. Time-resolved fluorescence spectroscopy revealed that CuInS₂/ZnS core/shell QDs apparently exhibited a slow decay compared with the CuInS₂ cores (214 ns for CuInS₂/ZnS QDs and 172 ns for CuInS₂ cores).

Because of the tunable near-infrared range emission, high stability and long lifetimes of the CuInS₂/ZnS QDs, they will be very useful in applications such as solar cell and biological imaging.

Keywords CuInS₂ · Semiconductor · Nanocrystals · Fluorescence · Lifetime

Abbreviations

QDs	Quantum dots
PL	Photoluminescence
NIR	Near-infrared
XRD	X-ray powder diffraction
TEM	Transmission electron microscopy
DAP	Donor–acceptor pair
ODE	1-Octadecene

Introduction

Semiconductor quantum dots (QDs) have attracted considerable interest over the past years because of their unique electronic and optical properties and potential applications, such as biomedical labeling (Bruchez et al. 1998; Chan and Nie 1998), optoelectronic devices (Colvin et al. 1994), and solar cells (Huynh et al. 2002; Pan et al. 2012). Early research in this area had been focused on the synthesis and optical characterization of the II–VI type (Peng and Peng

R. Zhang · P. Yang (✉)
School of Material Science and Engineering, University of Jinan, Jinan 250022, People's Republic of China
e-mail: mse_yangp@ujn.edu.cn

Y. Wang
The Cultivation Base for State Key Laboratory, Qingdao University, No. 308 Ningxia Road, Qingdao 266071, People's Republic of China

2001; Yang et al. 2011) and IV–VI type QDs (Ouyang et al. 2011) owing to their excellent physical properties. However, most of the QDs contain toxic elements (Cd, Pb, Hg, Te, As etc.), which limit their further applications in real world. For this reason, people turned their attentions to ternary I–III–VI compounds. As alternative materials, various I–III–VI type ternary colloidal QDs with less-toxic components including CuInS₂ (Zhong et al. 2008; Uehara et al. 2008; Li et al. 2009, 2011; Nam et al. 2011a, b; Kim et al. 2012; Park and Kim 2011; Pons et al. 2010; Song and Yang 2012; Yue et al. 2010; Xie et al. 2009; Pan et al. 2008; Castro et al. 2004; Li and Teng 2010), CuInSe₂ (Nose et al. 2009), CuGaS₂ (Wang et al. 2011), AgInS₂ (Hamanaka et al. 2011), and AgGaS₂ (Uematsu et al. 2010) have been proposed by many research groups, and their properties and applications have been studied.

CuInS₂ with a direct band gap of 1.5 eV is of particular interest in photovoltaic applications because its direct bandgaps with energies well matched to the solar spectrum, high absorption coefficients, high radiation stability, and low toxicity. Recent reports have demonstrated the potential of using CuInS₂ QDs in photovoltaic devices with power conversion efficiencies approaching ~5 % (Weil et al. 2010). In addition, CuInS₂ QDs exhibit color-tunable emission ranging from the visible to near-infrared (NIR) region, which is very important in biomedical labeling and light-emitting diodes. Due to all these interesting features, colloidal synthesis routes to these QDs have been intensively developed in the last years. Li et al. (2009) demonstrated the interest of highly luminescent CuInS₂/ZnS core/shell QDs as fluorescent probes for in vivo biological imaging. Pons and co-workers studied the toxicity of the CuInS₂/ZnS QDs for NIR emitting by comparing the inflammatory response of the axillary LN induced by different doses of CuInS₂/ZnS and CdTeSe/CdZnS QDs, and they demonstrated that CuInS₂/ZnS QDs presented a much reduced in vivo local acute toxicity compared to CdTeSe/CdZnS QDs (Pons et al. 2010). Yang and co-workers demonstrated that highly luminescent CuInS₂/ZnS core/shell QDs had been used for the fabrication white QD-based light-emitting diodes (Song and Yang 2012).

Several approaches for the production of CuInS₂ QDs have been explored, including the hot-injection (Park and Kim 2011; Pons et al. 2010; Xie et al. 2009), heating-up (Kim et al. 2012), solvothermal synthesis

(Yue et al. 2010; Nam et al. 2011a; Li and Teng 2010), thermolysis (Castro et al. 2004), and photochemical decomposition methods (Nairn et al. 2006). Among the approaches listed above, hot-injection and heating-up routes were mostly used. Although, the heating-up method is regarded as a great choice for the fabrication of CuInS₂ QDs on a large scale, the hot-injection method is considered to be a better way to fabricate mono-disperse-sized QDs. However, the synthetic methods have not been developed quite satisfactory so far because most of the obtained CuInS₂ QDs provided low luminescence efficiency and stability deficits.

To obtain CuInS₂ QD emitters with more efficiently photoluminescence (PL), several works on the synthesis of CuInS₂ QDs were employed. For instance, Zhong et al. reported a facile synthesis of CuInS₂ QDs by thermolysis of a mixed solution of CuAc, In(Ac)₃, and 1-dodecanethiol in a noncoordinating solvent 1-octadecene (ODE) (Zhong et al. 2008). Uehara et al. (2008) improved the PL of CuInS₂ QDs by intentionally introducing crystal defects related to the Cu deficiency in QD through a highly off-stoichiometric composition from CuInS₂. Intentional off-stoichiometric CuInS₂ QDs can possess more donor or acceptor states, thereby providing more radiative sites for the donor–acceptor pair recombination and consequently enhancing their PL efficiency. Recently, Hamanaka et al. reported that the PL of CuInS₂ QDs was ascribed to the deep surface trap recombination (Hamanaka et al. 2008). Another efficient means of enhancing PL efficiency and photostability of CuInS₂ QDs is by the surface passivation via growing a shell of a higher band gap material to form core–shell structured QDs. ZnS is typically chosen as a shell material for CuInS₂ core passivation. Recently, Peng et al. reported size-dependent CuInS₂/ZnS core/shell QDs which were synthesized by a hot-injection method exhibited a maximum PL efficiency of ~30 % and tunable emissions of 500–950 nm (Xie et al. 2009). Reiss et al. synthesized highly luminescent CuInS₂/ZnS core/shell QDs with a maximum efficiency of ~60 % and tunable emissions of 595–812 nm via a heat-up method (Li et al. 2009). Park and Kim (2011) reported a large improvement in PL intensity with the maximum PL efficiency of 65 % from 625 nm emitting CuInS₂/ZnS core/shell QDs, in which the ZnS overlayer was generated through a cation exchange reaction. Li et al. (2011) published an efficient synthesis of CuInS₂ QDs with strong PL and a high

chemical yield in excess of 90 % by an ODE-free heating method. The PL efficiency can be improved from 5–10 % in as-prepared QDs to more than 80 % for a core/shell structure with a few monolayers of CdS or ZnS. The dramatic improvement in PL can be ascribed to suppression of a nonradiative recombination process associated with surface-related traps. Very recently, Kim et al. (2012) explored the effect of nonstoichiometry and surface modification with zinc acetate and fatty acid on the PL of the QDs, and the PL efficiency of the CuInS₂/ZnS QDs reached up to 70 %. As seen from the above reports, PL efficiency and emission color tunability of CuInS₂/ZnS QDs seem to be strongly dependent on their own synthetic details. Consequently, it remains a major goal to fabricate highly luminescent stable CuInS₂ QDs.

In this paper, CuInS₂ QDs were successfully prepared in noncoordinating solvent ODE via reaction between the chlorides of the corresponding metals and elemental sulfur as starting compounds in the presence of oleylamine and dodecanethiol. Compared with the report in literature (Li et al. 2009), the QDs were created at relative low temperature because of the difference of starting materials. The PL properties of CuInS₂ QDs were improved by both controlling copper stoichiometry and surface modification. The resulting core/shell QDs exhibited a dramatically increase in PL efficiency and stability, with the maximum PL efficiency up to 39 %. With the experimental conditions varying, the PL spectra can be tuned from the red to NIR. In addition to absorption and PL spectroscopy, the PL properties of the obtained CuInS₂ and CuInS₂/ZnS core/shell QDs were studied by time-resolved PL spectroscopy. The QDs exhibited high stability in an organic solvent.

Experimental sections

Chemicals

Indium (III) chloride (InCl₃, 99.995 %), copper (I) chloride (CuCl, ≥97.0 %), sulfur powder (S, 99 %), oleylamine (OAm, 97 %), and zinc stearate (Zn(SA)₂, ≥97.0 %) were supplied by Shanghai Chemical Reagent Company. 1-Dodecanethiol (DDT, 99.9 %), and ODE (90 %) were purchased from Sigma-Aldrich. Hexane, methanol, and sulfur

powder (S, 99 %) were taken from Tianjin Chemical Reagent Company. All the chemicals were used as received without any further purification.

Synthesis of CuInS₂ QDs

High-quality CuInS₂ QDs were synthesized in organic solvent at elevated temperatures based on recently reported methods (Xie et al. 2009). For a typical synthesis of CuInS₂ QDs with a Cu/In ratio of 1/1, 9.9 mg of CuCl, 22.1 mg of InCl₃, 2 ml of OAm, and 5 ml of ODE were loaded into a three-neck flask. This mixture was heated to 150 °C and kept at this temperature for 30 min under an N₂ atmosphere. When the solution was heated to 170 °C, 1 ml 1-dodecanethiol was added into reaction solution. At this moment, the color of the solution became slight yellow. The solution was then heated to 180 °C and a solution of 6.4 mg of sulfur dissolved in 1 ml of ODE was swiftly injected into the flask. The mixture was stirred at this temperature for 1 min to allow the particle growth. Finally, the reaction was quenched by rapidly cooling the flask in a water bath. CuInS₂ QDs with Cu/In ratios of 1/2, 1/4, and 1/8 were synthesized under the same reaction conditions as above except the ratio of precursors.

In situ synthesis of CuInS₂/ZnS QDs

CuInS₂ QDs were synthesized as mentioned above. Then, a Zn precursor solution was prepared by dissolving 63.3 mg of zinc stearate in 4 ml of ODE at 120 °C. This solution was injected into the reaction flask including CuInS₂ QDs (without purification) under an N₂ atmosphere. After that, the mixture was heated to 180 °C and then maintained at this temperature for a certain time (from 1 to 10 min), after which the reaction was quenched by rapidly cooling the flask in a water bath.

Purification of QDs

The QD dispersions were diluted by the addition of hexane. The as-prepared CuInS₂ cores and CuInS₂/ZnS core/shell QDs were precipitated with an excess of ethanol, and centrifuged at 10,000 rpm for 10 min. This process was repeated three times. The resulting products were finally redispersed in hexane.

Apparatus

The low-resolution transmission electron microscopy (TEM) observations were carried out using a JEM-1011 transmission electron microscope with an acceleration voltage of 100 kV. The specimen was prepared by depositing a drop of a dilute hexane solution of the final products on a carbon film-coated copper grid and dried at room temperature. HR-TEM images were taken on a JEM-2100F transmission electron microscope with an acceleration voltage of 200 kV. X-ray powder diffraction (XRD) patterns were obtained via a Bruker D8 X-ray powder diffractometer using a Cu K α target. The UV–Visible absorption and the PL spectra of the QDs were acquired at room temperature by using a Hitachi U-4100 UV–Vis–NIR spectrophotometer and a Hitachi F-4600 fluorescence spectrophotometer, respectively. The PL efficiencies of the QDs in solution were estimated by comparing with standard solutions, such as a rhodamine 6G (efficiency of $\sim 95\%$) ethanol solution (Karstens and Kobs 1980; Grabolle et al. 2009). The PL lifetimes of samples were obtained using a time-correlated single-photon-counting spectrofluorometer system (Fluorocube-01, JY-IBH, Horiba). All initial QD samples were characterized without any size sorting at room temperature.

Results and discussion

The effect of Cu/In molar ratio of the starting materials were extraordinarily critical on the PL properties of resulting QDs. Table 1 illustrates the preparation conditions and properties of CuInS₂ and CuInS₂/ZnS QDs. Figure 1 shows the absorption and PL spectra of CuInS₂ QDs prepared using different Cu/In molar ratios. With the Cu/In molar ratio decreasing, the corresponding absorption and PL peak were blue-shifted (with PL peak wavelengths of 795.4 nm for Cu/In = 1/1 and 701.3 nm for Cu/In = 1/8). On one hand, this systematic blue-shift can be attributed to the size difference of the QDs, which has direct relation with quantum confinement and has been widely investigated, ultimately affecting QD band gap. TEM observation indicated the variation of the QDs with Cu/In molar ratios (see TEM characterization). On the other, the blue-shift of PL spectra can be ascribed primarily to the variation of the Cu/In composition-dependent band gap in CuInS₂ QDs as discussed in previous reports

(Uehara et al. 2008; Nam et al. 2011b; Kim et al. 2012), where this phenomenon is generally attributable to the lowering in energy of valence band edge due to the hybridization between Cu *d* and S *p* orbitals in Cu-deficient material, ultimately leading to a widening of band gap.

It was noted that the absorption and PL spectra of all resulting CuInS₂ QDs revealed a very broad feature, with the bandwidth of 123–135 nm. Compared with a small Stokes-shift (<100 meV) observed from II–VI-based QDs, the emission peaks of CuInS₂ QDs are significantly red-shifted versus their absorption peaks. The accurate determination of Stokes-shift might be difficult due to the broad features of absorption and PL spectra. Such a broad emission and a large Stokes-shift could not be ascribed to the carrier recombination between quantized electron–hole levels, but to the presence of intragap states, which can be internal and/or surface defects sites. The exact emission mechanism of these quantized CuInS₂ QDs appears to be still under debate. A commonly accepted transition mechanism is so-called donor–acceptor pair (DAP) recombination (Nam et al. 2011b; Li et al. 2009; Castro et al. 2004), where a sulfur vacancy (V_S), an interstitial copper (Cu_i), and an indium substituted at a copper site (In_{Cu}) are likely to act as donor states, with a copper vacancy (V_{Cu}), an indium interstitial (In_i), and a copper substituted at an indium site (Cu_{In}) as acceptor states. The particular type of these donor and acceptor states

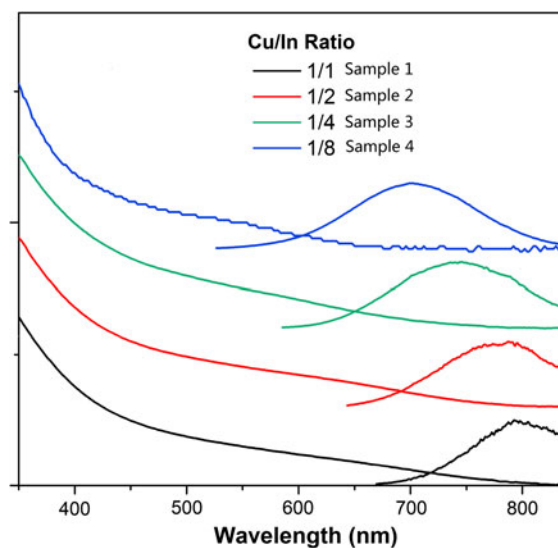


Fig. 1 Absorption and PL spectra of CuInS₂ QDs prepared at different Cu/In molar ratios

would depend on the stoichiometry of CuInS_2 , i.e., Cu-rich versus In-rich phases (Castro et al. 2004; Nose et al. 2009; Hofhuis et al. 2008), determining the dominant DAP recombination pathway. An alternative transition from a quantized conduction band state to a localized intragap state is also proposed by Li et al. (2011). The broad feature of the emission band is characteristic of defect-related radiative transition like the case of CuInS_2 QDs. Meanwhile, the broad feature of the emission band might be caused by QD size inhomogeneity. However, the QD size of all resulting QDs was uniform (see TEM observation), further conforming the defect-related recombination mechanism as discussed above. The PL efficiency of CuInS_2 QDs with Cu/In = 1/1, 1/2, 1/4, and 1/8 were measured to be 1.6, 3.4, 6.9, and 8.3 %, respectively. Such an increasing trend in PL efficiency with more Cu-deficient QDs is consistent with the work done by Uehara et al. (2008) and Nam et al. (2011b). Intentionally, preparing Cu-deficient QDs can provide a higher density of Cu-related defect states, thereby providing higher probability of carrier recombination and consequently enhancing their PL efficiency.

Figure 2a shows the TEM image of representative CuInS_2 QDs (sample 1) prepared using a Cu/In molar ratio of 1/1, whose size was uniform with an average diameter of 4.0 nm, while the average diameter of CuInS_2 QDs (sample 4) prepared using a Cu/In molar ratio of 1/8 was widely dispersed is 3.4 nm as shown in Fig. 2c. ZnS is the most appropriate shell material for the surface passivation of I–III–VI type QDs because of its large band gap (3.6 eV for the bulk material) for the formation of a type I band alignment with CuInS_2 , small lattice mismatch (2–3 %), and crystallographic similarity between CuInS_2 and ZnS, and its chemical stability and nontoxic character. To further improve PL efficiency, we coated the CuInS_2 QDs with a ZnS shell through a facile in situ fabrication process. Upon ZnS shell overcoating on CuInS_2 QDs, the average diameters of samples 5 and 7 ($\text{CuInS}_2/\text{ZnS}$ core/shell QDs) were increased into 4.3 and 3.6 nm, respectively, as shown in Fig. 2b, d. After surface modification, a noticeable improvement in the uniformity of size distribution of the QDs was observed by the TEM images. The thickness of ZnS shell could be roughly estimated to be 0.3–0.5 nm (approximately 1.0–1.5 ZnS monolayers (Borchert et al. 2002)).

Figure 3 shows the XRD patterns of CuInS_2 (sample 4 prepared using a Cu/In molar ratio of 1/8)

and $\text{CuInS}_2/\text{ZnS}$ QDs (sample 7 prepared by sample 4 as cores). A close analysis of the XRD patterns indicates that the QDs do not possess a chalcopyrite structure. We then simulated diffraction patterns using the lattice parameters previously reported for wurtzite CuInS_2 and found it well matched with our XRD patterns, indicating the CuInS_2 QDs reveals a wurtzite structure (Pan et al. 2008). After the CuInS_2 QDs were overcoated with the ZnS shell, all peaks exhibited a notable shift toward higher angles, closely approaching the characteristic peak positions of bulk wurtzite ZnS. The XRD peak shift of surface-modified QDs implies ZnS shell layer formation on CuInS_2 QDs. A similar behavior has been observed for other core/shell systems, such as CdSe/ZnS and CdSe/CdS (Dabbousi et al. 1997; Peng et al. 1997). The broad peaks of the patterns suggest the small size nature of the samples which is consistent with the above TEM images shown in Fig. 2c, d.

Figure 4 shows the evolution of absorption and PL spectra of $\text{CuInS}_2/\text{ZnS}$ QDs with time. (a) The absorption spectra of sample 5, (b) the PL spectra of sample 5, (c) the PL spectra of sample 6, and (d) the PL spectra of sample 5. The absorption and PL spectra of CuInS_2 cores are shown in Fig. 4 for comparison. As seen from the absorption spectra (Fig. 4a), the absorption shoulders of all QD samples were located at similar wavelengths. This result reveals that the band gap of original core QD remained largely unchanged after formation of ZnS, which can rule out the possibility of diffusion of Zn ion into CuInS_2 core or partial interfacial alloying at core/shell occurs during shell coating. Compared with their original CuInS_2 core QDs, a significant blue-shift in PL emission was observed during the initial stage of a shell growth time (i.e., 1 min), and then emission peaks shifted to the blue gradually up to 5 min of shell growth time and did not shift any more with the reaction time prolonged to 10 min as shown in Fig. 4b. Figure 4c, d shows the PL spectra of $\text{CuInS}_2/\text{ZnS}$ QDs at different reaction times. The formation of $\text{CuInS}_2/\text{ZnS}$ core/shell nanostructures resulted in a dramatic enhancement of the PL intensity. Before the growth of a ZnS shell, the CuInS_2 core QDs revealed relatively low PL efficiency (typically below 8 %). Being coated with a ZnS shell, the PL efficiency of the resulting core/shell QDs increased substantially with the highest PL efficiency reached to 39 %, more than five times. Upon overcoating with

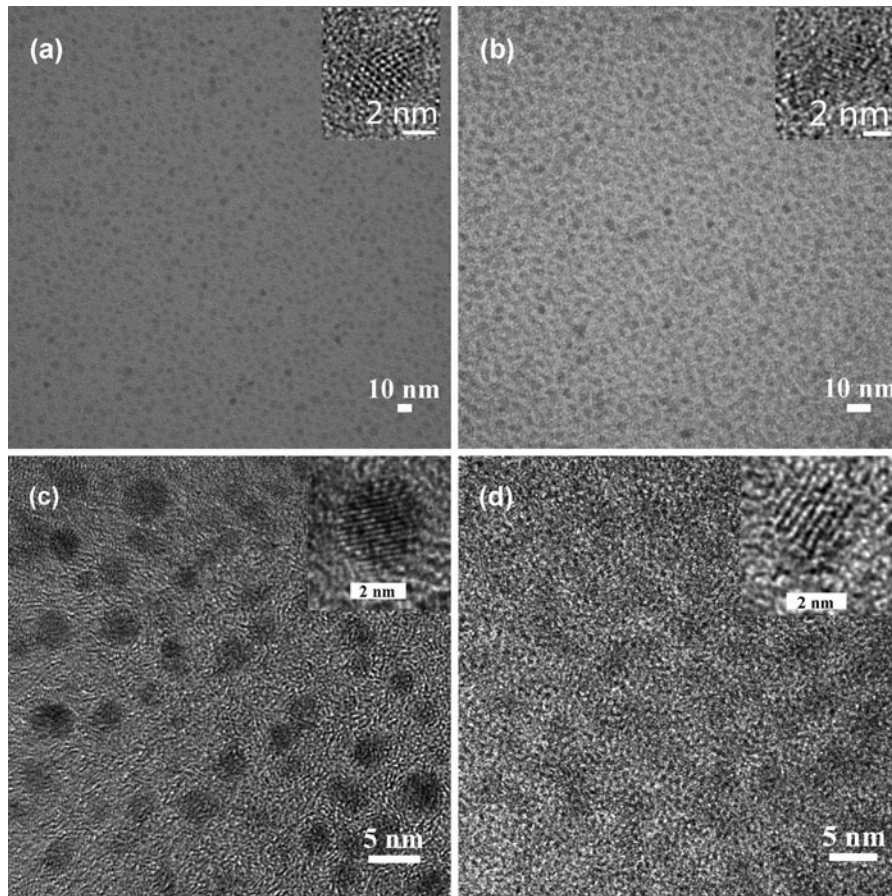


Fig. 2 TEM images of CuInS_2 and $\text{CuInS}_2/\text{ZnS}$ samples. **a** Sample 1, CuInS_2 cores prepared using Cu/In molar ratio of 1/1. **b** Sample 5, $\text{CuInS}_2/\text{ZnS}$ QDs prepared using sample 1.

c Sample 4, CuInS_2 cores prepared using Cu/In molar ratio of 1/8. **d** Sample 7, $\text{CuInS}_2/\text{ZnS}$ QDs prepared using sample 4

ZnS shell, the surface of CuInS_2 cores would be well passivated by the effective elimination of the surface defects, resulting in such an enhanced efficiency.

Being coated with a ZnS shell, the blue-shift of PL spectra was observed, even though the degree of blue-shift of $\text{CuInS}_2/\text{ZnS}$ QDs was varied depending on their preparation conditions. Various descriptions on the origin of blue-shift in PL spectra have been suggested, such as size decrease by cation exchange (Park and Kim 2011), surface etching (Li et al. 2011; Kim et al. 2012), partial interfacial alloying of CuInS_2 core with ZnS (Nam et al. 2011a), or surface reconstruction (Li et al. 2009) during ZnS shell growth. However, our absorption spectra (Fig. 4a) could rule out the possibility of Zn diffusion-associated blue-shift since the band gap widening of core/shell QDs was not observed. Surface reconstruction

might be one of the answers, but hard to claim without an appropriate theoretical or experimental understanding. Very recently, Nam et al. (2011b) proposed a new hypothesis to explain the substantially blue-shifted emission by suggesting an alternative radiative recombination pathway of CB-to- V_{Cu} instead of DAP recombination. Thus, the blue-shift in PL emission of CuInS_2 QDs after ZnS shell coating was not fully investigated and is still under debate.

To understand the mechanism underlying the dramatic improvement in PL efficiency in core/shell particles, we studied the PL dynamics of the CuInS_2 QDs before and after shell growth. It has been discussed that the intrinsic defects, size-dependent band gap, and surface defects are all involved in the PL emission (Zhang 1997). Different radiative lifetimes may correspond to different electron-hole recombination

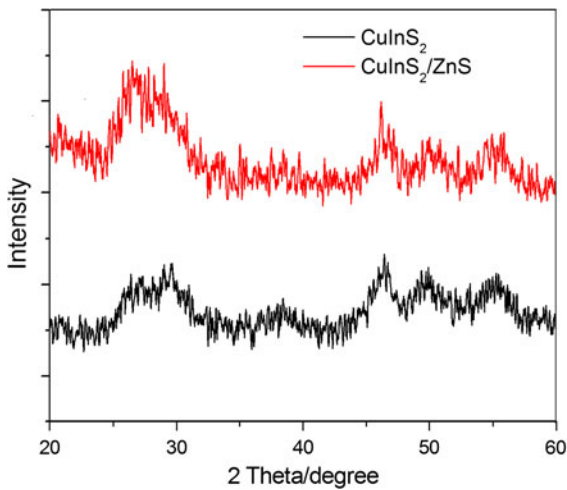


Fig. 3 XRD patterns of CuInS₂ (sample 4) and CuInS₂/ZnS QDs (sample 7). Both samples 4 and 7 revealed wurtzite structure

mechanisms. Figure 5 demonstrates the PL decay curves of the CuInS₂ cores prepared using a Cu/In molar ratio of 1/8 and the corresponding CuInS₂/ZnS core/shell QDs. The PL decay curves can be well fitted by a triexponential function:

$$F(t) = A + B_1 \exp(-t/\tau_1) + B_2 \exp(-t/\tau_2) + B_3 \exp(-t/\tau_3)$$

where $\tau_1(\tau_2, \tau_3)$ represents the time constants; and $B_1(B_2, B_3)$ represents the amplitudes of the decay components at $t = 0$. Average lifetime τ is calculated as follows:

$$\tau = (B_1 \tau_1^2 + B_2 \tau_2^2 + B_3 \tau_3^2) / (B_1 \tau_1 + B_2 \tau_2 + B_3 \tau_3).$$

These fitted values of the parameters $B_1, B_2, B_3, \tau_1, \tau_2, \tau_3$, and τ are summarized in Table 2, with τ_1 ranging from 29 to 31 ns, τ_2 ranging from 2 to 5 ns, and τ_3 ranging from 175 to 216 ns. In all the

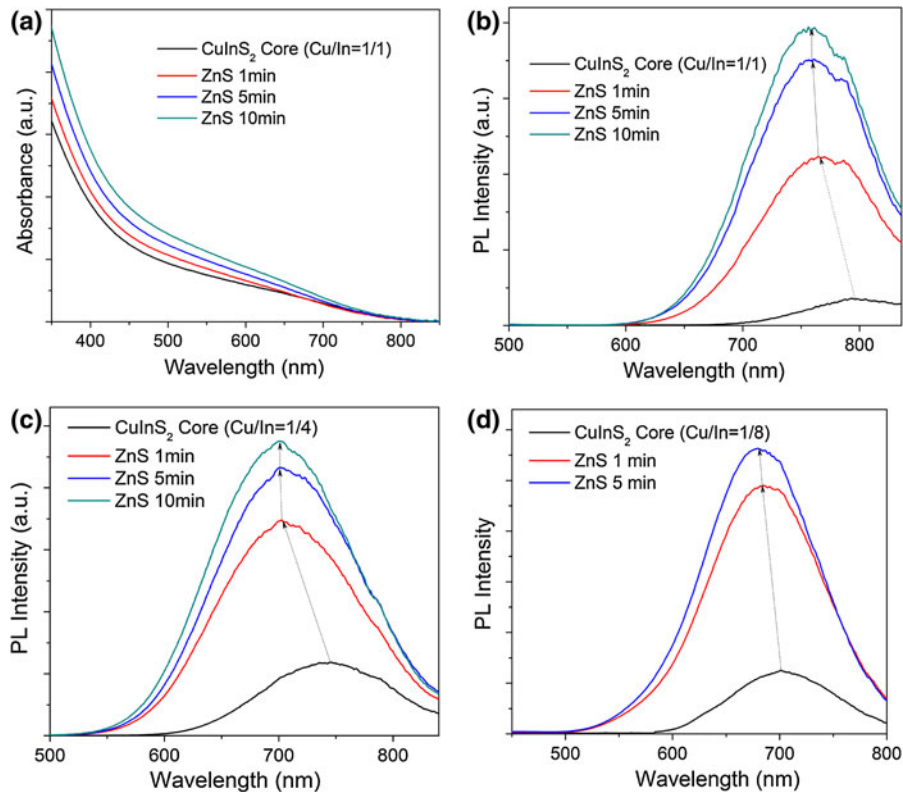


Fig. 4 Evolution of absorption and PL spectra of CuInS₂/ZnS core-shell QDs during preparation. **a** Absorption spectra of sample 5. **b** PL spectra of sample 5. **c** PL spectra of sample 6.

d PL spectra of sample 5. The absorption and PL spectra of CuInS₂ cores are shown for comparison

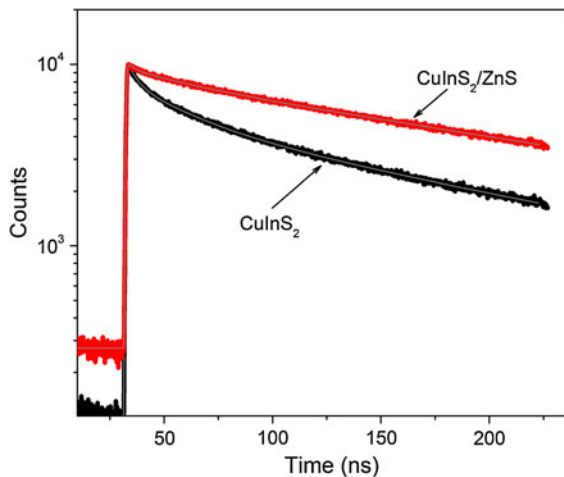


Fig. 5 PL decay curves (measured at the maximum of the emission peak, $\lambda_{\text{ex}} = 371$ nm) of CuInS₂ cores (sample 4) and CuInS₂/ZnS core-shell QDs (sample 7). Reproduced curves for data shown in Table 2 are plotted as *thin gray lines*

wavelengths of the CuInS₂ and CuInS₂/ZnS QDs, the amplitude B_3 with PL decay lifetime of 175–216 ns accounts for a large amount (88–97 %) of the total PL emission spectra. Previous PL decay investigations of binary II–VI QDs (such as CdSe (Crooker et al. 2003) and CdTe (Yang and Murase 2010)) revealed that the radiative time of binary II–VI QDs has a universal biexponential time distribution. Typically, a shorter lifetime is on the time scale of several nanoseconds, and a longer lifetime is tens of nanoseconds. The shorter lifetime is associated with the intrinsic recombination of initially populated core states, while the longer lifetime is considered to originate from surface states. In our case, the two radiative lifetimes τ_1 and τ_2 may be assigned to intrinsic recombination of initially populated core states and surface states, respectively. The long luminescence lifetime (hundreds of

nanoseconds) is correlated to DAP recombination, which can also explain the broad emission peaks. Such results were consistent with the previous PL decay investigations on CuInS₂ QDs (Zhong et al. 2008; Kim et al. 2012). There are three types of PL radiative mechanisms in the PL spectrum of the as-prepared CuInS₂ and CuInS₂/ZnS QDs, and the PL emission mainly originates from the intrinsic DAP recombination. It was noticed that the CuInS₂/ZnS core/shell QDs apparently showed a slower decay compared with the original CuInS₂ QDs. The fast decay component was minimized after the surface modification through formation of ZnS shell. This demonstrates the reduction of the surface defects, which can also be deduced from the improvement of PL efficiencies after overcoating with ZnS (Table 1).

The degradation of QDs is always related to the diffusion of oxygen from the surroundings. We firstly check the stability of CuInS₂ QDs, The PL of samples 1 and 2 quenched after preparation for 1 days. However, PL intensity of sample 4 almost remained unchanged after 10 days as shown in Figure 6. This indicates the molar ratios of Cu/In affect the stability of the QDs. As for a Cu/In molar ratio of 1/4 (sample 3), the situation is similar with the molar ratio of 1/8. The result indicates that the surface oxidation can be suppressed significantly with the decreasing amount of Cu content. Figure 6 shows the evolution of PL intensity of CuInS₂ cores (sample 4) CuInS₂/ZnS core/shell QDs (samples 5 and 7) in organic solvents. By monitoring the PL properties, it was identified that the PL efficiency decreased gradually with time. The degradation rate of the CuInS₂/ZnS core/shell QDs was slow compared with the corresponding CuInS₂ ones under ambient conditions. Therefore, the growth of ZnS shell not only dramatically enhanced the PL efficiency of the CuInS₂ QDs but also improved their

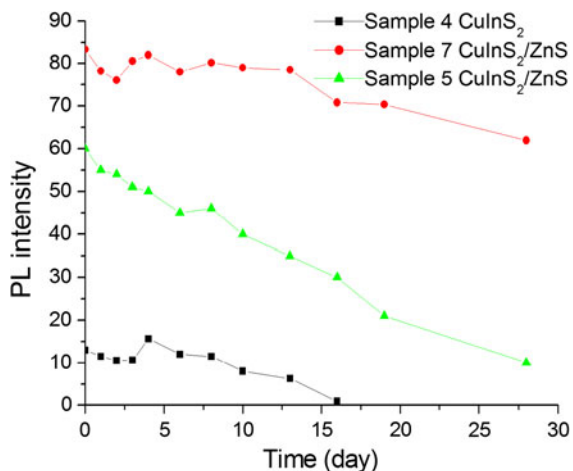
Table 1 Preparation conditions and properties of CuInS₂ and CuInS₂/ZnS QDs

Sample	Composition	Cu/In molar ratio	Core	PL peak wavelength (nm)	PL efficiency (%)	Average diameter (nm)
1	CuInS ₂	1/1	N/A	795.4	1.6	4.0
2	CuInS ₂	1/2	N/A	790.1	3.4	3.9
3	CuInS ₂	1/4	N/A	745.6	6.9	3.6
4	CuInS ₂	1/8	N/A	701.3	8.3	3.4
5	CuInS ₂ /ZnS	1/1	Sample 1	760.1	10.1	4.3
6	CuInS ₂ /ZnS	1/4	Sample 3	705.6	24.3	3.8
7	CuInS ₂ /ZnS	1/8	Sample 4	685.5	39.0	3.6

The reaction time for the preparation of samples 5–7 is 5 min

Table 2 Components B_1 , B_2 , and B_3 ; time constants τ_1 , τ_2 and τ_3 ; and average lifetime τ of CuInS_2 core (sample 4) and the corresponding $\text{CuInS}_2/\text{ZnS}$ QDs (sample 7)

Sample	B_1 (%)	τ_1 (ns)	B_2 (%)	τ_2 (ns)	B_3 (%)	τ_2 (ns)	τ_2 (ns)
CuInS_2	10.65	30.33	1.3	4.39	88.05	175.41	172.38
$\text{CuInS}_2/\text{ZnS}$	2.18	29.07	0.16	2.95	97.66	215.03	214.47

**Fig. 6** Evolution of PL intensity of CuInS_2 cores (sample 4) and $\text{CuInS}_2/\text{ZnS}$ core-shell QDs (samples 5 and 7) in organic solutions

stability. These results are consistent with a $\text{CuInS}_2/\text{ZnS}$ core/shell QD structure with a complete coating of a ZnS shell.

Conclusions

Low-toxic and environment-benign colloidal CuInS_2 QDs have been prepared via a simple and reliable synthesis method using air-stable compounds. The PL properties of the obtained QDs are strongly depended on Cu/In molar ratios. As a result of a widened band gap from Cu-deficient CuInS_2 QDs, a systematic blue-shift of emission was observed from QDs with a higher degree of Cu deficiency. In addition, with large copper deficiency generated intentionally, the PL intensity of CuInS_2 QDs was improved due to the enhanced internal defect-related emission. Subsequently, a ZnS shell overcoating on the surface of CuInS_2 QDs was conducted. Owing to the effective surface passivation by ZnS shell, the PL efficiency and stability increased substantially with a maximum value of 39 % and

emission wavelength tunable from 670 to 800 nm. In addition to absorption and PL spectroscopy, the PL properties of the obtained CuInS_2 and $\text{CuInS}_2/\text{ZnS}$ core/shell QDs were studied by time-resolved PL spectroscopy. The observed lifetimes of several hundreds of nanoseconds together with the comparably broad emission peaks indicated that the PL emission of CuInS_2 and $\text{CuInS}_2/\text{ZnS}$ QDs mainly originated from the donor-acceptor defects.

Acknowledgments This work was supported in part by the Program for Taishan Scholars from Shandong province government, projects from National Natural Science Foundation of China (21071061), Natural Science Foundation of Shandong Province (ZR2010EZ001 and ZR2009FM072), Outstanding Young Scientists Foundation Grant of Shandong Province (BS2010CL004 and BS2012CL004), the Research Foundation from University of Jinan (XKY0911 and XKY1006), and the Doctor Foundation from University of Jinan (XBS1015 and XBS1027).

References

- Borchert H, Haubold S, Haase M, Weller H (2002) Investigation of ZnS passivated InP nanocrystals by XPS. *Nano Lett* 2(2):151–154
- Bruchez MJr, Moronne M, Gin P, Weiss S, Alivisatos AP (1998) Semiconductor nanocrystals as fluorescent biological labels. *Science* 281(5385):2013–2016
- Castro SL, Bailey SG, Raffaele RP, Banger KK, Hepp AF (2004) Synthesis and characterization of colloidal CuInS_2 nanoparticles from a molecular single-source precursor. *J Phys Chem B* 108(33):12429–12435
- Chan WCW, Nie S (1998) Quantum dot bioconjugates for ultrasensitive nonisotopic detection. *Science* 281:2016–2018
- Colvin VL, Schlamp MC, Alivisatos AP (1994) Light-emitting diodes made from cadmium selenide nanocrystals and a semiconducting polymer. *Nature* 370:354–357
- Crooker SA, Barrick T, Hollingsworth JA, Klimov VI (2003) Multiple temperature regimes of radiative decay in CdSe nanocrystal quantum dots: intrinsic limits to the dark-exciton lifetime. *Appl Phys Lett* 82(17):2793–2795
- Dabbousi BO, Rodriguez-Viejo J, Mikulec FV, Heine JR, Mattoussi H, Ober R, Jensen KF, Bawendi MG (1997) (CdSe)ZnS core-shell quantum dots: synthesis and characterization of a size series of highly luminescent nanocrystallites. *J Phys Chem B* 101(46):9463–9475

- Grabolle M, Spieles M, Lesnyak V, Gaponik N, Eychmuller A, Resch-Genger U (2009) Determination of the fluorescence quantum yield of quantum dots: suitable procedures and achievable uncertainties. *Anal Chem* 81(15):6285–6294
- Hamanaka Y, Kuzuya T, Sofue T, Kino T, Ito K, Sumiyama K (2008) Defect-induced photoluminescence and third-order nonlinear optical response of chemically synthesized chalcopyrite CuInS₂ nanoparticles. *Chem Phys Lett* 466:176–180
- Hamanaka Y, Ogawa T, Tsuzuki M (2011) Photoluminescence properties and its origin of AgInS₂ quantum dots with chalcopyrite structure. *J Phys Chem C* 115:1786–1792
- Hofhuis J, Schoonman J, Goossens A (2008) Elucidation of the excited-state dynamics in CuInS₂ thin films. *J Phys Chem C* 112(38):15052–15059
- Huynh WU, Dittmer JJ, Alivisatos AP (2002) Hybrid nanorod-polymer solar cells. *Science* 295:2425–2427
- Karstens T, Kobs K (1980) Rhodamine B and Rhodamine 101 as reference substances for fluorescence quantum yield measurements. *J Phys Chem* 84(14):1871–1872
- Kim YK, Ahn SH, Chung K, Cho YS, Choi CJ (2012) The photoluminescence of CuInS₂ nanocrystals: effect of non-stoichiometry and surface modification. *J Mater Chem* 22:1516–1520
- Li TL, Teng H (2010) Solution synthesis of high-quality CuInS₂ quantum dots as sensitizers for TiO₂ photoelectrodes. *J Mater Chem* 20:3656–3664
- Li L, Daou TJ, Texier I, Chi TTK, Liem NQ, Reiss P (2009) Highly luminescent CuInS₂/ZnS core/shell nanocrystals: cadmium-free quantum dots for in vivo imaging. *Chem Mater* 21(12):2422–2429
- Li L, Pandey A, Werder DJ, Khanal BP, Pietryga JM, Klimov VI (2011) Efficient synthesis of highly luminescent copper indium sulfide-based core/shell nanocrystals with surprisingly long-lived emission. *J Am Chem Soc* 133:1176–1179
- Nairn JJ, Shapiro PJ, Twamley B, Pounds T, von Wandruszka R, Fletcher TR, Williams M, Wang C, Norton MG (2006) Preparation of ultrafine chalcopyrite nanoparticles via the photochemical decomposition of molecular single-source precursors. *Nano Lett* 6(6):1218–1223
- Nam DE, Song WS, Yang H (2011a) Facile, air-insensitive solvothermal synthesis of emission-tunable CuInS₂/ZnS quantum dots with high quantum yields. *J Mater Chem* 21:18220–18226
- Nam DE, Song WS, Yang H (2011b) Noninjection, one-pot synthesis of Cu-deficient CuInS₂/ZnS core/shell quantum dots and their fluorescent properties. *J Colloid Interface Sci* 361:491–496
- Nose K, Omata T, Otsuka-Yao-Matsuo S (2009) Colloidal synthesis of ternary copper indium diselenide quantum dots and their optical properties. *J Phys Chem C* 113(9):3455–3460
- Ouyang J, Schuurmans C, Zhang Y, Nagelkerke R, Wu X, Kingston D, Wang ZY, Wilkinson D, Li C, Leek DM, Tao Y, Yu K (2011) Low-temperature approach to high-yield and reproducible syntheses of high-quality small-sized PbSe colloidal nanocrystals for photovoltaic applications. *ACS Appl Mater Interfaces* 3:553–565
- Pan D, An L, Sun Z, Hou W, Yang Y, Yang Z, Lu Y (2008) Synthesis of Cu–In–S ternary nanocrystals with tunable structure and composition. *J Am Chem Soc* 130(17):5620–5621
- Pan Z, Zhang H, Cheng K, Hou Y, Hua J, Zhong X (2012) Highly efficient inverted Type-I CdS/CdSe core/shell structure QD-sensitized solar cells. *ACS Nano* 6(5):3982–3991
- Park J, Kim SW (2011) CuInS₂/ZnS core/shell quantum dots by cation exchange and their blue-shifted photoluminescence. *J Mater Chem* 21:3745–3750
- Peng ZA, Peng X (2001) Formation of high-quality CdTe, CdSe, and CdS nanocrystals using CdO as precursor. *J Am Chem Soc* 123(1):183–184
- Peng X, Schlamp MC, Kadavanich AV, Alivisatos AP (1997) Epitaxial growth of highly luminescent CdSe/CdS core/shell nanocrystals with photostability and electronic accessibility. *J Am Chem Soc* 119(30):7019–7029
- Pons T, Pic E, Lequeux N, Cassette E, Bezdetnaya L, Guillemin F, Marchal F, Dubertret B (2010) Cadmium-free CuInS₂/ZnS quantum dots for sentinel lymph node imaging with reduced toxicity. *ACS Nano* 4(5):2531–2538
- Song WS, Yang H (2012) Efficient white-light-emitting diodes fabricated from highly fluorescent copper indium sulfide core/shell quantum dots. *Chem Mater* 24:1961–1967
- Uehara M, Watanabe K, Tajiri Y, Nakamura H, Maeda H (2008) Synthesis of CuInS₂ fluorescent nanocrystals and enhancement of fluorescence by controlling crystal defect. *J Chem Phys* 129:134709
- Uematsu T, Doi T, Torimoto T, Kuwabata S (2010) Preparation of luminescent AgInS₂–AgGaS₂ solid solution nanoparticles and their optical properties. *J Phys Chem Lett* 1:3283–3287
- Wang YHA, Zhang X, Bao N, Lin B, Gupta A (2011) Synthesis of shape-controlled monodisperse wurtzite CuIn_xGa_{1-x}S₂ semiconductor nanocrystals with tunable band gap. *J Am Chem Soc* 133:11072–11075
- Weil BD, Connor ST, Cui Y (2010) CuInS₂ solar cells by air-stable ink rolling. *J Am Chem Soc* 132(19):6642–6643
- Xie R, Rutherford M, Peng X (2009) Formation of high-quality I-III-VI semiconductor nanocrystals by tuning relative reactivity of cationic precursors. *J Am Chem Soc* 131(15):5691–5697
- Yang P, Murase N (2010) Preparation-condition dependence of hybrid SiO₂-coated CdTe nanocrystals with intense and tunable photoluminescence. *Adv Funct Mater* 20(8):1258–1265
- Yang P, Ando M, Taguchi T, Murase N (2011) Highly luminescent CdSe/Cd_xZn_{1-x}S quantum dots with narrow spectrum and widely tunable wavelength. *J Phys Chem C* 115:14455–14460
- Yue W, Han S, Peng R, Shen W, Geng H, Wu F, Tao S, Wang M (2010) CuInS₂ quantum dots synthesized by a solvothermal route and their application as effective electron acceptors for hybrid solar cells. *J Mater Chem* 20:7570–7578
- Zhang JZ (1997) Ultrafast studies of electron dynamics in semiconductor and metal colloidal nanoparticles: effects of size and surface. *Acc Chem Res* 30(10):423–429
- Zhong H, Zhou Y, Ye M, He Y, Ye J, He C, Yang C, Li Y (2008) Controlled synthesis and optical properties of colloidal ternary chalcogenide CuInS₂ nanocrystals. *Chem Mater* 20(20):6434–6443